



HAL
open science

On elemental and isotopic fractionation of noble gases in geological fluids by molecular diffusion

Hai Hoang, Khac Hieu Ho, Anne Battani, Magali Pujol, Guillaume Galliero

► To cite this version:

Hai Hoang, Khac Hieu Ho, Anne Battani, Magali Pujol, Guillaume Galliero. On elemental and isotopic fractionation of noble gases in geological fluids by molecular diffusion. *Geochimica et Cosmochimica Acta*, 2021, 315, pp.172-184. 10.1016/j.gca.2021.09.002 . hal-03962184

HAL Id: hal-03962184

<https://univ-pau.hal.science/hal-03962184>

Submitted on 5 Jan 2024

HAL is a multi-disciplinary open access archive for the deposit and dissemination of scientific research documents, whether they are published or not. The documents may come from teaching and research institutions in France or abroad, or from public or private research centers.

L'archive ouverte pluridisciplinaire **HAL**, est destinée au dépôt et à la diffusion de documents scientifiques de niveau recherche, publiés ou non, émanant des établissements d'enseignement et de recherche français ou étrangers, des laboratoires publics ou privés.



Distributed under a Creative Commons Attribution - NonCommercial 4.0 International License

26 is shown to be unable to provide reasonable results, confirming recent experimental and
27 numerical works. As expected, it has been noticed that the kinetic theory relation provides a
28 reasonable estimate of the isotopic fractionation in gas whereas it deteriorates in water and in
29 oil. Finally, using the previous findings, we propose a simple and predictive scheme for the
30 isotopic fractionation of noble gases in all studied geo-fluids which is noticeably better than
31 both the square-root and the kinetic theory relations.

32

33 **Keywords:** Noble gas, isotopes, fractionation, diffusion, molecular simulation

34 **1. Introduction**

35 Noble gases have been widely used as natural tracers to characterize the storage,
36 migration and origin of fluids in geological environments (Ozima et al., 2002; Ballentine et al.
37 2002; Burnard, 2013). Interestingly, they are chemically and biologically inert and therefore
38 are only fractionated, i.e. partially separated, by physical processes (Ozima et al., 2002).
39 Among the existing physical processes, molecular diffusion is expected to significantly
40 induce noble gases kinetic fractionation in geo-fluids (Marty, 1984; Prinzhofer et al., 2000;
41 Ballentine et al., 2002). Such a kinetic fractionation, simply called fractionation in the
42 following, emerges from the relative differences between molecular diffusion of noble gases
43 when migrating into a fluid. However, its precise quantification and its modeling are still open
44 for debates (Bourg and Sposito, 2008; Tyroller et al., 2014; Tyroller et al., 2018; Seltzer et al.,
45 2019), wider than the noble gas community (Watkins et al., 2017; Wanner and Hunkeler,
46 2019). The purpose of this article is to provide new insights on the quantification of noble
47 gases fractionation by molecular diffusion in various geo-fluids, in particular in oil and gas.

48 One of the main reasons for the debate to still be ongoing is the difficulty to
49 experimentally quantify the elemental and even more the isotopic fractionation of noble gases
50 due to molecular diffusion in geo-fluids (Jähne et al., 1987; Tempest and Emerson, 2013;
51 Tyroller et al., 2014, Tyroller et al., 2018; Seltzer et al., 2019). Furthermore, these
52 experiments are mostly limited to what occurs in water at standard conditions. As an
53 alternative to experiments, molecular dynamics (MD) simulations (Allen and Tildesley, 2017;
54 Frenkel and Smit, 2001) proved to be an effective tool for diffusion coefficients estimation in
55 fluids. In particular, this numerical tool was already used to successfully estimate the
56 elemental and isotopic fractionation of noble gases by molecular diffusion in water (Bourg
57 and Sposito, 2008). With progresses in molecular modeling, MD simulations are now able to
58 provide accurate results for the equilibrium and transport properties of various geo-fluids

59 under subsurface conditions, including noble gases, natural gases and oil (Leach, 2001;
60 Martin and Siepmann, 1998; Siu et al., 2012; Marrink and Tieleman, 2013; Hoang et al.,
61 2017; Hoang et al., 2019).

62 A significant number of theoretical and empirical models are already proposed in the
63 literature to quantify mass diffusion coefficients in various environments (Chapman and
64 Cowling, 1981; Poling et al., 2001; Cussler, 2009). However, quite surprisingly, the most
65 common approach to quantify the fractionation by molecular diffusion, whether isotopic or
66 elementary, is simply based on the evaluation of the inverse of the square root of the mass
67 ratios of the two species considered whatever the geo-fluids and the pressure and temperature
68 conditions (Ballentine et al., 2002; Watkins et al., 2017; Wanner and Hunkeler, 2019). This
69 simple relationship (called in the following the square root law) although theoretically correct
70 for isotopic fractionation under low-density gas condition or in the limit of ultra-tight porous
71 medium (Marty, 1984; Ballentine et al., 2002) only, consistently describes noble gases
72 elemental fractionation in aqueous fluids under standard conditions (Jähne et al., 1987).
73 Nevertheless, recent experimental studies and numerical simulations showed that the square
74 root law tends to strongly overestimate noble gas isotopes fractionation in aqueous fluids
75 (Bourg and Sposito, 2008; Tempest and Emerson, 2013; Tyroller et al., 2014; Tyroller et al.,
76 2018; Seltzer et al., 2019). Similar findings have been noticed for other solute elements such
77 as alkali and alkali earth metals, halides and CO₂, in both liquid water and silicate melts
78 (Richter et al., 2006; Zeebe, 2011; Bourg et al., 2010; Watkins et al., 2017; Wanner and
79 Hunkeler, 2019).

80 Thus, to rationalize all the results on noble gases, we propose in this work to
81 systematically study the limits and capabilities of the various fractionation models applied to
82 them in various geo-fluids, including not only water as already looked after in the seminal
83 work of Bourg and Sposito (2008), but also gas (methane) and oil (n-hexane), using molecular

84 simulations data. As it will be shown, this approach allowed us to explain why the square root
85 law holds well for elemental fractionation and led us to propose a generic semi-empirical
86 model able to provide a good estimate of noble gas isotopic fractionation by diffusion
87 whatever the geo-fluids and the thermodynamic conditions considered.

88 The article is organized as follows: in section II, we provide details on existing
89 fractionation models and on numerical details of molecular simulations. The results obtained
90 from molecular simulations and theoretical models are presented and discussed in sections III
91 and IV, respectively. Finally, the main results of this study are summarized in section V,
92 which is the conclusion.

93 **2. Theory and Simulation**

94 **2.1. Kinetic Fractionation by molecular diffusion**

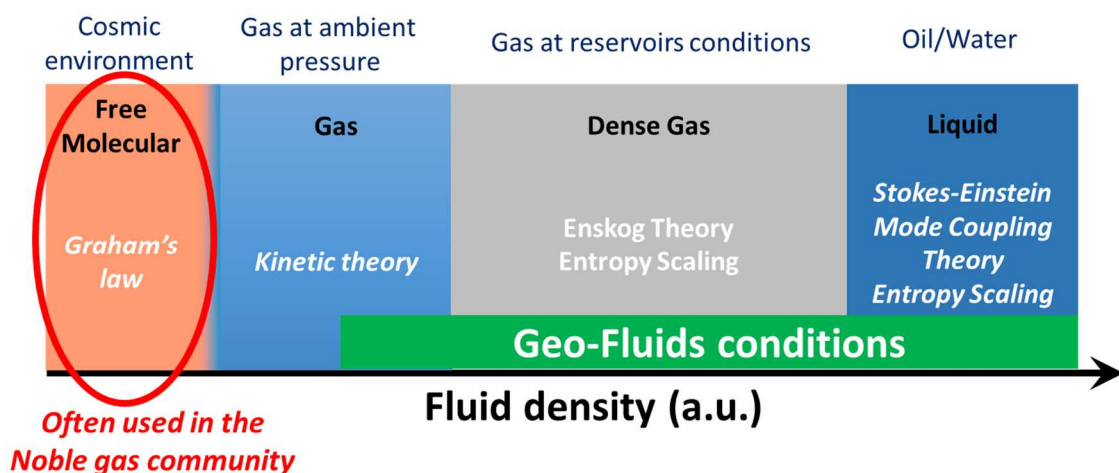
95 Molecular diffusion processes are expected to induce both isotopic and elemental
96 kinetic fractionation of trace elements in geo-fluids (Marty, 1984; Watkins et al., 2017;
97 Wanner and Hunkeler, 2019). Such a fractionation is simply due to a difference in the relative
98 migration velocity, by molecular diffusion, of the components when advection is absent. It is
99 a complex and coupled transient phenomenon occurring only when the system is out of
100 equilibrium, i.e. when the compositions of the considered components are not constant over
101 space (Cussler, 2009). As noble gases are present under trace in geo-fluids, the problem is
102 simpler than the general one covering all ranges of concentration. For a diluted component i ,
103 the migration velocity by molecular diffusion is simply characterized by its self-diffusion
104 coefficient, D_i . As a consequence, the relative fractionation between two diluted species i and
105 j in a solvent, is fully defined by the fractionation coefficient α , which writes as:

$$106 \quad \alpha[i/j] = \frac{D_i}{D_j} \quad (1)$$

107 Thus, the problem of quantifying the noble gases fractionation by molecular diffusion
 108 reduces to the knowledge of the self-diffusion coefficients of noble gases in the considered
 109 geo-fluids under the studied pressure and temperature conditions. However, self-diffusion
 110 measurements are difficult to achieve (Jähne et al., 1987; Tempest and Emerson, 2013;
 111 Tyroller et al., 2014; Tyroller et al., 2018; Seltzer et al., 2019), even more in subsurface
 112 conditions (i.e. high pressures). Hence, an accurate model of noble gas self-diffusion in
 113 geological fluids under subsurface conditions would be more than welcome.

114 2.2. Molecular diffusion theory

115 Many theoretical and empirical models are proposed in the literature to estimate the
 116 molecular diffusion of gas molecules in a fluid (Chapman and Cowling, 1981; Poling et al.,
 117 2001; Cussler, 2009; Watkins et al., 2017; Wanner and Hunkeler, 2019). However, their
 118 ability to provide accurate results is often limited to a specific range of thermodynamic
 119 conditions which can be classified into four main regimes: free molecular regime, kinetic
 120 theory regime, intermediate density regime, and liquid regime. Figure 1 shows these diffusion
 121 regimes and the models which are, *a priori*, the most suitable for each regime. In the
 122 following sections, these models are briefly presented and their ability to predict the noble gas
 123 elemental and isotopic fractionation in geo-fluids is discussed.



125 *Figure 1: The various regimes of molecular diffusion for different fluid conditions and the*
126 *corresponding theoretical models.*

127

128

129 **2.2.1. Free-molecular regime**

130 The “free-molecular” regime corresponds to the situation where the mean-free path of
131 the molecules in the fluid phase is larger than the size of the confining solid structure (pore,
132 tube, chamber...). Fluid molecules in this regime collide with the walls of the solid structure
133 more frequently than with other fluid molecules. Such a regime is typically observed at near
134 vacuum conditions when the confining structure is large, as in cosmic environment. Under
135 sub-surface conditions it may occur only in extremely tight porous medium as the mean free
136 path of gas under surface conditions is about tenth of nanometers, and this value strongly
137 decreases with pressure. Under these very specific conditions, the molecular diffusion of a
138 species i is proportional to the thermal velocity of the molecules, and therefore is inversely
139 proportional to the square root of its molecular mass, M_i , i.e.

$$140 \quad D_i \propto M_i^{-1/2} \quad (2)$$

141 This relationship is often referred to as Graham’s law. In such conditions, the
142 fractionation coefficient α between component j and i , is simply given by:

$$143 \quad \alpha[i/j] = \left(\frac{M_j}{M_i}\right)^{1/2} \quad (3)$$

144 This square root law is widely used to predict both elemental and isotopic fractionation of
145 noble gases due to molecular diffusion in geological environments (Ballentine et al., 2002),
146 despite its very limited applicability in sub-surface environments from the theoretical point of
147 view as pointed out previously.

148 Rather surprisingly, experiments and molecular simulations showed that noble gas
 149 elemental fractionation in liquid water is well described by equation (3) (Jähne et al., 1987;
 150 Bourg and Sposito, 2008). However, recent studies, including experiments (Tempest and
 151 Emerson, 2013; Tyroller et al., 2014; Tyroller et al., 2018; Seltzer et al., 2019) and
 152 simulations (Bourg and Sposito, 2008), evidenced that this relation strongly overestimates
 153 noble gases isotope fractionation in water.

154 **2.2.2. Gas regime**

155 The “gas” regime corresponds to the cases where the average distance between the
 156 fluid molecules is much larger than the size of the molecules, while their mean free paths are
 157 smaller than the size of the confining solid structure. Such conditions typically correspond to
 158 gases at standard conditions. In this regime, the molecular diffusion is controlled by binary
 159 collisions between molecules, and is consistently described by the kinetic theory (Chapman
 160 and Cowling, 1981). In such conditions, the self-diffusion coefficient of a noble gas i depends
 161 on both its own size and its own mass, but also on those of the solvent, in the following way:

$$162 \quad D_i \propto \left[\frac{R_i + R_S}{2} \right]^{-2} \times \mu_i^{-1/2} \quad (4)$$

163 where R_i is the radius of the noble gas molecule, R_S is the radius of the solvent molecule,
 164 $\mu_i = (M_i \times M_S)/(M_i + M_S)$ is the reduced mass where M_S is the molecular mass of solvent.

165 In such a regime, the fractionation coefficient between two noble gas isotopes i and j is
 166 given by:

$$167 \quad \alpha[i/j] = \left(\frac{\mu_j}{\mu_i} \right)^{1/2} = \left(\frac{M_j}{M_i} \right)^{1/2} \times \left(\frac{M_i + M_S}{M_j + M_S} \right)^{1/2} \quad (5)$$

168 It is interesting to notice that such a relation tends to equation (2) when the molecular mass of
 169 the solvent is large compared to the one of the studied noble gas isotopes as the second term
 170 in the right-hand side of equation (5) tends to unity. The elemental fractionation coefficient
 171 between noble gases i and j can be deduced as well from equation (4) which leads to:

172
$$\alpha[i/j] = \left(\frac{\mu_j}{\mu_i}\right)^{1/2} \times \left(\frac{R_j+R_s}{R_i+R_s}\right)^2 \quad (6)$$

173 Although the kinetic theory provides a simple and explicit expression to compute both
 174 elemental and isotopic fractionation of noble gases in gases, it is less applied than equation (2)
 175 in subsurface environment (Marty, 1984; Ballentine et al., 2002).

176 **2.2.3. Dense gas regime**

177 The “dense” gas regime is defined as the regime for which the fluid molecules mean
 178 free path is of the order of the molecule size. Such conditions typically correspond to what
 179 occurs in natural gases under reservoir conditions, i.e. under high pressures. In this regime,
 180 the molecular diffusion of gas molecules is rather complex as the collision dynamics is
 181 strongly correlated. Many theories exist to estimate molecular diffusion in such a regime, like
 182 the Enskog theory and its variants (Kincaid et al., 1988; Kincaid et al., 1994) or like the more
 183 recent entropy scaling law (Samanta et al., 2001; Samanta et al., 2004). Both lead to relations
 184 similar to equation (4) for the molecular diffusion with a correction term depending on the
 185 local molecular structure, e.g. given by the radial distribution function (Allen and Tildesley,
 186 1987), around the species of interest.

187 Thus, the Enskog theory and the entropy scaling law both lead to an isotopic
 188 fractionation coefficient equal to the one obtained by the kinetic theory, i.e. described using
 189 equation (5), whereas the elemental fractionation coefficient is provided by a relation similar
 190 to equation (6) modulated by a structural correction:

191
$$\alpha[i/j] = \left(\frac{\mu_j}{\mu_i}\right)^{1/2} \times \left(\frac{R_j+R_s}{R_i+R_s}\right)^2 \times C \quad (7)$$

192 where C is a correction term which depends both on thermodynamics conditions and on
 193 species involved.

194 **2.2.4. Liquid regime**

195 The “liquid” regime corresponds to the situation in which the gas molecules are
 196 solubilized in a dense fluid, i.e. the molecules are in close contact and strongly interact. These
 197 conditions are typically those found in a liquid. In such a regime, the diffusion coefficient of a
 198 dilute component i can be modeled by the generalized Stokes-Einstein relation (Bhattacharyya
 199 and Bagchi, 2000; Ali et al., 2001):

$$200 \quad D_i = \frac{k_B T}{\zeta} \quad (8)$$

201 where ζ is the friction coefficient of the liquid acting on the gas molecules. As shown by the
 202 mode coupling theory, this friction coefficient can be expressed as a combination of various
 203 contributions due to the binary collision dynamics, the continuum collision dynamics and the
 204 collective relaxation of the liquid. It typically leads to an isotopic fractionation coefficient
 205 which can be approximated by:

$$206 \quad \alpha[i/j] = \left(\frac{M_j}{M_i}\right)^\beta \quad (9)$$

207 in which β is a parameter varying from 0 to 0.2, as confirmed by molecular simulations
 208 results (Bourg and Sposito, 2008; Bourg et al., 2010; Zeebe, 2011). The case of $\beta = 0$
 209 corresponds to the Brownian dynamics limit, i.e. no isotope fractionation.

210 Regarding elemental fractionation, the situation is even more complex. As a first
 211 approximation, one can rely on the widely used Wilke-Chang correlation for estimating the
 212 diffusion coefficient of noble gases (Wilke and Chang, 1955). By assuming so, the elemental
 213 fractionation coefficient becomes:

$$214 \quad \alpha[i/j] = \left(\frac{V_j}{V_i}\right)^{0.6} \quad (10)$$

215 where V_i is the molar volume of species i at a boiling point under normal conditions. It is
 216 interesting to point out that $\left(\frac{V_j}{V_i}\right)^{0.6} \approx \left(\frac{R_j}{R_i}\right)^2$, because the molar volume is closely related to the
 217 cube of the molecular size.

218 It is worth pointing out that equation (9) predicts a small isotopic fractionation of
 219 noble gases in liquids which is partially confirmed by recent experiments and simulations in
 220 water (Bourg and Sposito, 2008; Tyroller et al., 2018; Seltzer et al., 2019). In addition,
 221 elemental fractionation predicted by equation (10) indicates that fractionation is induced by
 222 the difference between the molecular sizes of the noble gases and not by the difference in
 223 their masses.

224

225

226 **2.3. Molecular dynamics Simulations**

227 **2.3.1. Molecular Modeling**

228 *Noble Gases in Gas and Oil*

229 To model the noble gases (Helium, Neon, Argon, Krypton and Xenon) and the n-
 230 alkanes (Methane and n-Hexane) studied in this work, we have used the Mie Chain Coarse-
 231 Grained (MCCG) force field developed by Hoang et al. (2017). This coarse-grained force
 232 field have exhibited in previous works an excellent capability to predict the equilibrium and
 233 transport properties of these compounds and their mixtures under sub-surface conditions
 234 (Hoang et al., 2017; Galliero et al., 2017; Hoang et al., 2019; Hamani et al., 2020).

235 A fluid molecule modeled by the MCCG consists on a simple homo-nuclear chain
 236 composed of N spheres which are freely and tangentially bonded, N being equal to one for all
 237 noble gases. Interactions between two non-bonded spheres i and j are described by using the
 238 Mie λ -6 potential:

$$239 \quad u_{Mie}(r_{ij}) = \left(\frac{\lambda_{ij}}{\lambda_{ij}-6} \right) \left(\frac{\lambda_{ij}}{6} \right)^{6/(\lambda_{ij}-6)} \varepsilon_{ij} \left[\left(\frac{\sigma_{ij}}{r_{ij}} \right)^{\lambda_{ij}} - \left(\frac{\sigma_{ij}}{r_{ij}} \right)^6 \right] \quad (11)$$

240 where r_{ij} is the distance between two spheres, ε_{ij} is the potential well depth, σ_{ij} is the
 241 collision diameter, and λ_{ij} is the exponent characterizing the repulsive interactions between

242 non-bonded spheres. Two adjacent particles in a chain are linked by a rigid bond with a bond
243 length equal to σ . Hence, the molecular representation with the MCGG force field requires
244 four parameters ($N, \lambda, \varepsilon, \sigma$) to fully describe a compound. These parameters were directly and
245 univocally determined from the critical temperature, one saturated liquid density, the acentric
246 factor and one saturated liquid reduced viscosity thanks to an extended corresponding states
247 principle (Hoang et al., 2017), except for Helium due to the quantum effect on the critical
248 properties (Gunn et al. 1966). The MCGG parameters of the studied species are reported in
249 Table S1 in the Supplementary Material (SM).

250 For the non-bonded interaction parameters between different species ($\varepsilon_{ij}, \sigma_{ij}, \lambda_{ij}$), the
251 classical Lorentz-Berthelot combining rules were used to determine ε_{ij} and σ_{ij} thanks to:

$$252 \quad \sigma_{ij} = \frac{(\sigma_{ii} + \sigma_{jj})}{2} \quad (12)$$

$$253 \quad \varepsilon_{ij} = \sqrt{\varepsilon_{ii}\varepsilon_{jj}} \quad (13)$$

254 and, an arithmetic average was used to obtain λ_{ij} (Hoang et al., 2017):

$$255 \quad \lambda_{ij} = \frac{\lambda_{ii} + \lambda_{jj}}{2} \quad (14)$$

256 *Noble Gases in Water*

257 The MCGG model is too simple to appropriately describe water molecules,
258 particularly hydrogen bonding. Thus, water molecules were modeled by using the extended
259 simple point charge (SPC/E) model, as it provides reasonable equilibrium and transport
260 properties under the studied temperature, $T=298.15\text{K}$ (Berendsen et al., 1987). A water
261 molecule represented by the SPC/E model is composed of two positively charged hydrogen
262 atoms and one negatively charged oxygen atom, in which the O-H bond and the H-O-H angle
263 are fixed at 0.1nm and at 109.47° , respectively. The noble gases used in combination with
264 water were modeled by the simple Lennard-Jones (LJ) sphere model, as usually used in
265 literature (Hirschfelder et al., 1954; Panagiotopoulos, 1989; Bourg and Sposito, 2008; Warr

266 et al., 2015), to be consistent with the SPC/E model. Details related to the interaction
267 parameters of these classical force fields are provided in Table S2 in the SM. The non-bonded
268 interaction parameters between unlike atoms ϵ_{ij} and σ_{ij} were determined by using the
269 classical Lorentz-Berthelot combining rules as given in equations (12) and (13). As already
270 reported in Bourg and Sposito (2008), these molecular force fields yield noble gases self-
271 diffusion coefficients in water in excellent agreement with experiments (Jähne et al., 1987),
272 see table S3 in the SM.

273

274

275 ***2.3.2. Numerical Details***

276 Molecular dynamics simulations were performed in the isobaric-isothermal ensemble
277 by using an in-house code (Hoang et al., 2017) for systems composed of noble gases in gas/oil
278 and using the LAMMPS code (Plimpton, 1995) for the noble gases in water. Simulation
279 systems consisted of cubic boxes composed of 1000 to 2000 molecules. Equations of motion
280 were integrated using the velocity-Verlet algorithm (Verlet, 1967), with a time-step of 1fs for
281 the noble gases in water and a value varying from 1fs to 3fs, depending on the mass of noble
282 gas isotopes, for the noble gases in gas and oil. Classical periodic boundary conditions were
283 applied in all directions. Temperature and pressure were kept constant using a Berendsen
284 thermostat and barostat, respectively (Berendsen et al., 1984). To constrain the bond length
285 and the bending angle, the classical RATTLE algorithm was employed (Andersen, 1983).
286 Non-bonded interactions were truncated at a cut-off radius $r_c = 3.5\sigma_{ij}$. Classical long-range
287 corrections were included for the Mie and LJ interaction (Allen and Tildesley, 2017; Frenkel
288 and Smit, 2001). Long-range electrostatic interactions were computed by using the Particle-
289 Particle and Particle-Mesh (PPPM) method (Deserno and Holm, 1998). To produce the
290 results, the MD simulations were performed in two successive steps. First, systems were

291 equilibrated for 3×10^6 time steps. Then, samplings were carried out during at least 6×10^6 time
292 steps.

293 Noble gases self-diffusion coefficients were computed by using the usual Einstein
294 relation (Allen and Tildesley, 2017):

$$295 \quad D = \lim_{t \rightarrow \infty} \frac{1}{6t} \langle [\mathbf{r}_i(t) - \mathbf{r}_i(0)]^2 \rangle \quad (15)$$

296 where, t is the time, $\langle \dots \rangle$ is the average over molecules and $\mathbf{r}_i(t)$ is the position of molecule i
297 at the time t . As noble gases are usually highly diluted in geo-fluids (of the order of 10^{-3} to 10^{-5}
298 in mole fraction (Ross, 2018)), equation (15) may provide simulation results with a poor
299 statistics and so to very large error bars. So, to improve the statistics, we used simulation
300 systems containing about 1%, in mole fraction, of noble gases, i.e. there are from 10 to 20
301 noble gas atoms in the simulation box. It was previously shown that such a concentration is
302 consistent with diluted conditions for the computation of self-diffusion coefficient (Hoang et
303 al., 2019). To further improve the statistic, the self-diffusion coefficients provided here
304 correspond to averages over 10 independent runs, and associated error bars correspond to
305 standard deviations.

306 **3. Results**

307 Molecular simulations were performed on noble gases (He, Ne, Ar, Kr and Xe) in: i)
308 water under ambient conditions at $T=298$ K and $P=0.1$ MPa, ii) methane (gas) and iii) n-
309 hexane (oil) under reservoir conditions at $T=423$ K and $P=50$ MPa and $T=323$ K and $P=10$
310 MPa, respectively. To compute the fractionation coefficient from equation (1), the self-
311 diffusion coefficients of the noble gases were computed using equation (15) as described in
312 section 2.3.2.

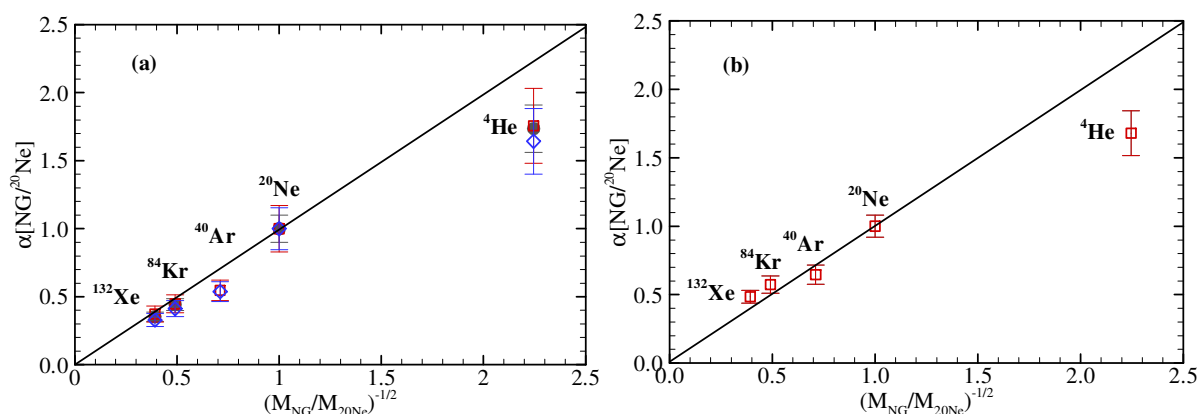
313 **3.1. Elemental Fractionation of Noble Gases**

314 Elemental fractionation coefficients of the major noble gases isotopes (^4He , ^{20}Ne , ^{40}Ar ,
315 ^{84}Kr and ^{132}Xe) in water, gas and oil are displayed in Fig. 2 and data are provided in table S4

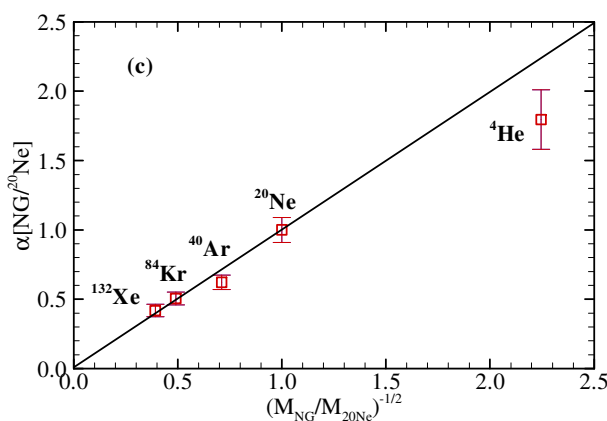
316 of the SM. ^{20}Ne is used as the reference (Jähne et al., 1987; Holz et al., 1994) and the
 317 fractionation coefficient of each noble gas is displayed relatively to the corresponding inverse
 318 square root of its molecular mass, i.e. $(M_{\text{NG}}/M^{20\text{Ne}})^{-1/2}$.

319 Figure 2a clearly shows a good agreement between the results obtained from our
 320 simulations and the available experiment and simulation data for the noble gases in water
 321 (Jähne et al., 1987, Bourg and Sposito, 2008). This confirms the consistency of our molecular
 322 simulation approach. Elemental fractionation coefficients of noble gases in the gas and the oil
 323 obtained from the MD simulations are shown on Figs. 2b and 2c. Even if small differences
 324 appear, it is interesting to notice that the results are very similar in gas and in oil and closely
 325 resemble to those obtained in water. This is particularly striking as the gas, oil and water
 326 studied significantly differ from each other in terms of molecular characteristics, pressure and
 327 temperature conditions and diffusion regime.

328



329



330 *Figure 2: Relationship between elemental fractionation $\alpha[NG/^{20}Ne]$ and the inverse of the*
331 *square root of the mass ratio $(M_{NG}/M_{^{20}Ne})^{-1/2}$. NG stands for the considered noble gas, and*
332 *M_{NG} for its mass. (a) In water at $T=298$ K and $P=0.1$ MPa. (b) In a gas (methane) at $T=423$*
333 *K and $P = 50$ MPa. (c) In an oil (n-hexane) at $T=323$ K and $P=10$ MPa. Black solid circles*
334 *correspond to experimental data (Jähne et al., 1987). Red open squares correspond to our*
335 *simulation data. Blue open diamonds correspond to the molecular simulation data of Bourg*
336 *and Sposito (2008). Lines correspond to equation (3).*

337

338 Another interesting, but surprising, result is that it appears clearly that the square root
339 law, equation (3), yields a good estimate of the fractionation coefficient for ^{40}Ar , ^{84}Kr and
340 ^{132}Xe , relatively to ^{20}Ne , not only in water as previously pointed out (Ballentine et al., 2002;
341 Bourg and Sposito, 2008), but also in gas and oil. However, such a relationship overestimates
342 $\alpha[^{4}He/^{20}Ne]$.

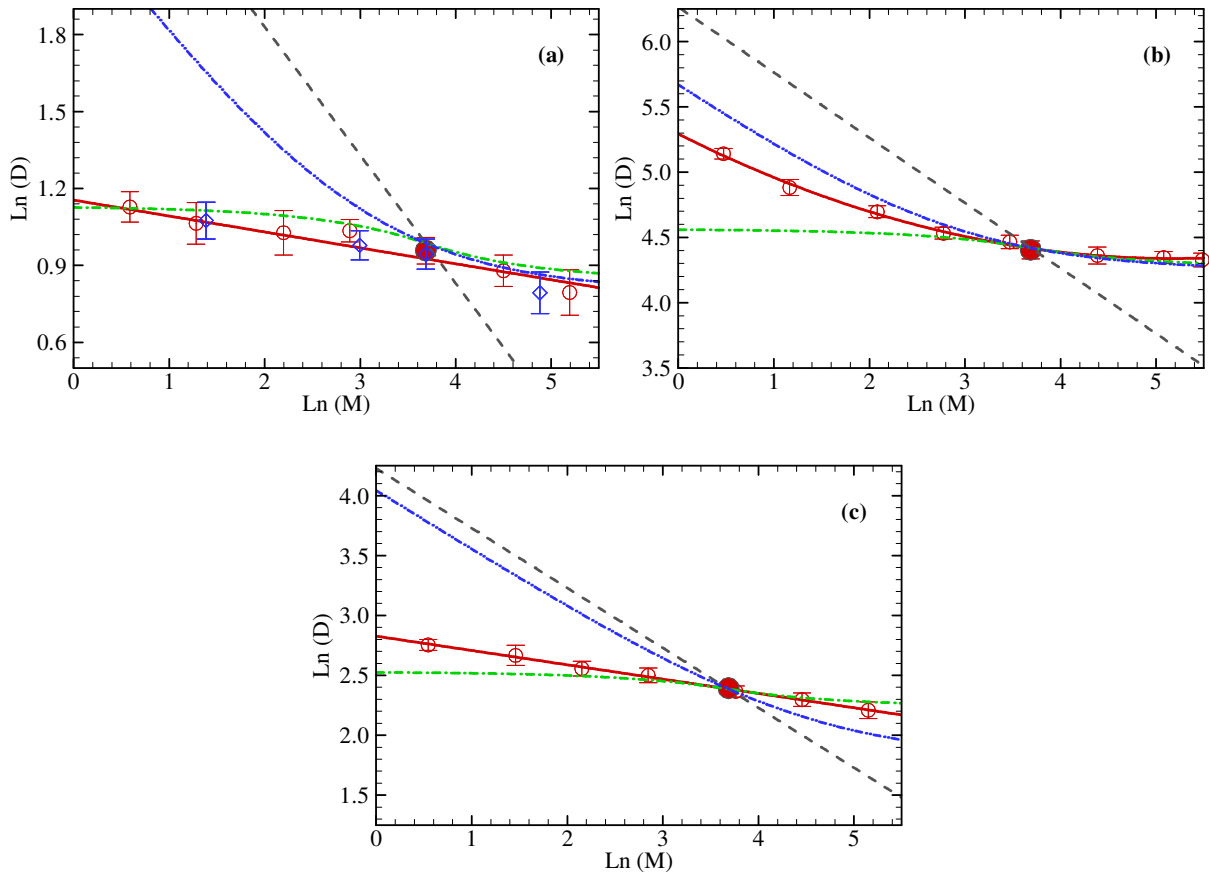
343 **3.2. Isotopic Fractionation of Noble Gases**

344 The accessible accuracy on diffusion coefficients using molecular dynamics
345 simulations is of the order on 7%, which is not precise enough to capture well the expected
346 isotopic fractionation in most cases. So, to reduce the statistical uncertainties, the self-
347 diffusion coefficients of noble gas isotopes were computed by using a fitting procedure based
348 on a strategy similar to the one employed by Bourg and Sposito (2008). More precisely, first
349 the self-diffusion coefficients of the studied noble gas for a wide range of masses (much
350 larger than that of real isotopes) were computed. This allows to enhance the dependence of
351 self-diffusion on the mass. Second, these values were fitted, as shown in Fig. 3 and Figs. S1-
352 S4, to deduce the self-diffusion coefficients of noble gas isotopes of interest.

353 Interestingly, the results of the simulations indicate that the dependence of self-
354 diffusion coefficient on the mass can be quantitatively described by a power law in water and

355 oil, consistently with previous simulation data in water (Bourg and Sposito, 2008), whereas it
 356 is not the case in gas, as illustrated in Fig. 3 for Argon and in Figs. S1-S4 in the
 357 Supplementary Material for the other noble gases. It is interesting to notice as well that our
 358 molecular simulation results in water are in good agreement with the ones provided by Bourg
 359 et al. (2008), see Fig. 3 and table S5 in the SM.

360



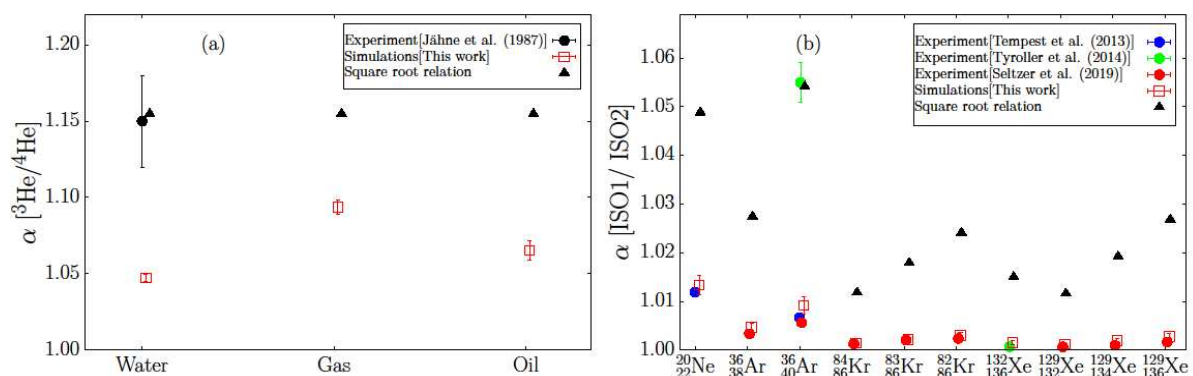
362

363 *Figure 3: Dependence of the logarithm of self-diffusion coefficient of Argon isotopes relatively to the*
 364 *logarithm of the mass. (a) In water at $T=298$ K and $P=0.1$ MPa. (b) In gas at $T = 423$ K and $P = 50$*
 365 *MPa. (c) In oil at $T = 323$ K and $P = 10$ MPa. Red open circles correspond to our simulation data.*
 366 *Blue open diamonds correspond to the simulation data of Bourg and Sposito (2008). Red solid circles*
 367 *correspond to the major isotope of Argon. Black dashed lines correspond to eq. (3), blue dashed-*
 368 *dotted-dotted lines to eq. (5) and green dashed-dotted line to eq. (17). Red full lines correspond to the*
 369 *linear (Figs. a and c) and second order polynomial (Fig. b) fit on the simulation data obtained from*
 370 *this work.*

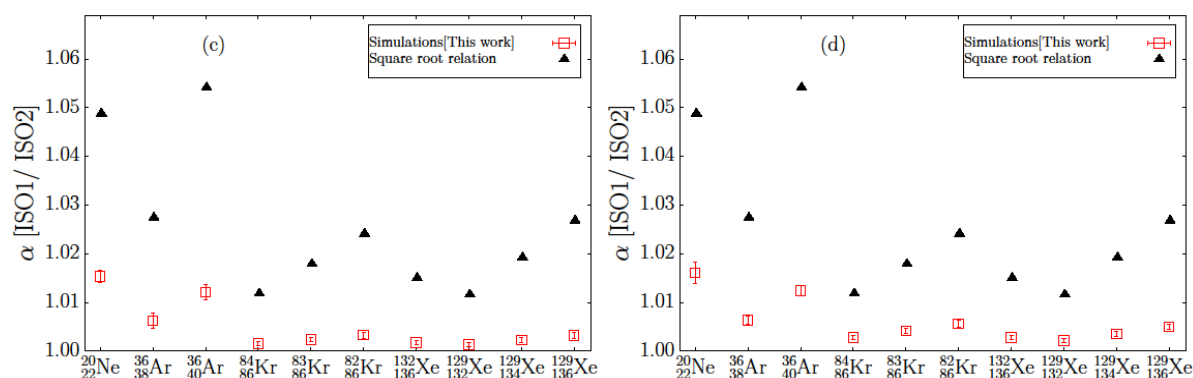
371

372 Isotopic fractionations in water obtained from the simulation results are shown in Fig.
 373 4a and 4b with data provided in Table S6 in the SM. Results indicate that the MD simulations
 374 are consistent with the experiments (Tempest and Emerson, 2013; Tyroller et al., 2014;
 375 Tyroller et al., 2018; Seltzer et al., 2019), except for $\alpha[{}^3\text{He}/{}^4\text{He}]$, see Fig. 3a, and for
 376 $\alpha[{}^{36}\text{Ar}/{}^{40}\text{Ar}]$, see Fig. 3b, obtained by Jähne et al. (1987) and Tyroller et al. (2014)
 377 respectively. Deviation between MD simulation and experiment for $\alpha[{}^3\text{He}/{}^4\text{He}]$ was already
 378 noticed by Bourg et al. (2008). It may be related to a quantum isotopic effect not taken into
 379 account in the MD simulations as pointed out by previous authors (Bourg and Sposito, 2008;
 380 de Magalhaes et al., 2017) or an experimental problem. Regarding the experiment data of
 381 Tyroller et al. (2014) for $\alpha[{}^{36}\text{Ar}/{}^{40}\text{Ar}]$, it is worth noticing that this data is not consistent with
 382 the experimental results obtained by Tempest and Emerson (2013) and Seltzer et al. (2019),
 383 the two latter being in good agreement with the MD simulations data, see Fig. 4b and table S5
 384 in the SM.

385



386



387 *Figure 4: (a) Isotopic fractionation of helium in various geo-fluids. (b) to (d) Isotopic*
388 *fractionation of noble gases (without helium) for classical noble gas isotopic ratios. ISO1 and*
389 *ISO2 respectively stand for numerator and denominator noble gas isotope and α the*
390 *fractionation coefficient for ISO1/ISO2 ratio. (b) in water at $T=298$ K and $P=0.1$ MPa. (c) in*
391 *gas at $T=423$ K and $P = 50$ MPa. (d) in oil at $T=323$ K and $P=10$ MPa.*

392

393 The isotopic fractionations of noble gases in the gas and the oil obtained from the MD
394 simulations are shown in Figs. 4a, 4c and 4d, respectively, and the data are provided in Tables
395 S7 and S8 in the SM. Interestingly, the trends and the order of magnitude of the fractionation
396 coefficients in both gas and oil are similar to what obtained in water. More precisely, the
397 noble gas isotope fractionation is more pronounced in gas, and even more in oil, than in water,
398 see Figs 4b, 4c and 4d, except for He, see Fig. 4a.

399 As can be deduced from Fig. 3 and Figs. S1-S4, the square root law is not appropriate
400 to capture the dependence of self-diffusion on noble gases masses. Hence, as shown in Fig. 4,
401 the square root law strongly overestimates the isotopic fractionation of noble gases in water,
402 gas and oil compared to MD simulations results. For the heaviest noble gases in gas and in
403 water, this overestimation can reach about one order of magnitude which confirms the limited
404 applicability of the square root law to quantify the noble gas isotope fractionation in geo-
405 fluids (Ballentine et al. 2002; Bourg and Sposito, 2008; Watkins et al., 2017; Wanner and
406 Hunkeler, 2019).

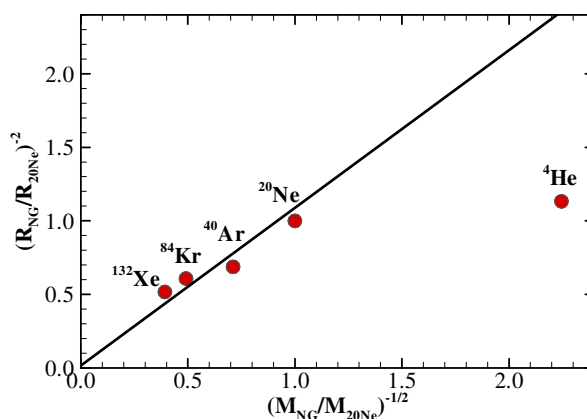
407 **4. Discussion**

408 **4.1. Elemental Fractionation of Noble Gases**

409 It has been shown that the square root law, equation (3), is able to provide a
410 quantitative estimate of the elemental fractionation of ^{40}Ar , ^{84}Kr and ^{132}Xe , relatively to ^{20}Ne ,
411 in all geo-fluids studied in this work (water, gas, oil). This result is rather surprising as such a

412 relation should only hold in the free-molecular diffusion regime, see section 2.2, whereas the
 413 studied solvent corresponds to the dense gas and the liquid diffusion regimes. Indeed, from
 414 equations (7) and (10), one would expect that elemental noble gases fractionation depends on
 415 their molecular radius ratio, and, to a less extent (in particular in a liquid solvent), to their
 416 mass ratio. More precisely, from equations (7) and (10), it is expected that the fractionation
 417 coefficient should be linked to the square of the inverse of the molecular radius ratio, i.e. to
 418 $(R_i/R_j)^{-2}$ and, to a less extent, to the square root of the inverse of the molecular mass ratio,
 419 i.e. $(M_i/M_j)^{-1/2}$.

420 The fact that the mass ratio alone is sufficient to capture well the elemental
 421 fractionation of noble gas whatever the geo-fluids probably indicates that noble gases
 422 molecular radius and mass are strongly correlated. Such a link is confirmed in Fig. 5, which
 423 displays $(R_{NG}/R_{20Ne})^{-2}$ against $(M_{NG}/M_{20Ne})^{-1/2}$ for the major noble gas isotopes (data are
 424 provided in Table S9 in the SI). This figure, which is very similar to Fig. 2, clearly shows that,
 425 for Ne, Ar, Kr and Xe, there is a nearly linear link between the square of the inverse of the
 426 molecular radius and the square root of the inverse of the molecular mass. For helium, $(R^{4He}/R^{20Ne})^{-2}$
 427 is below this linear line, which is consistent with the simulation results on elemental
 428 fractionation, see Fig. 2.



429

430 *Figure 5: Relationship between molecular size and molecular mass for major noble gas*
431 *isotopes. R stands for molecular radius, M for mass and NG for the considered noble gas*
432 *isotope. Solid line corresponds to a linearly fitting between (^{20}Ne , ^{40}Ar , ^{84}Kr and ^{132}Xe).*

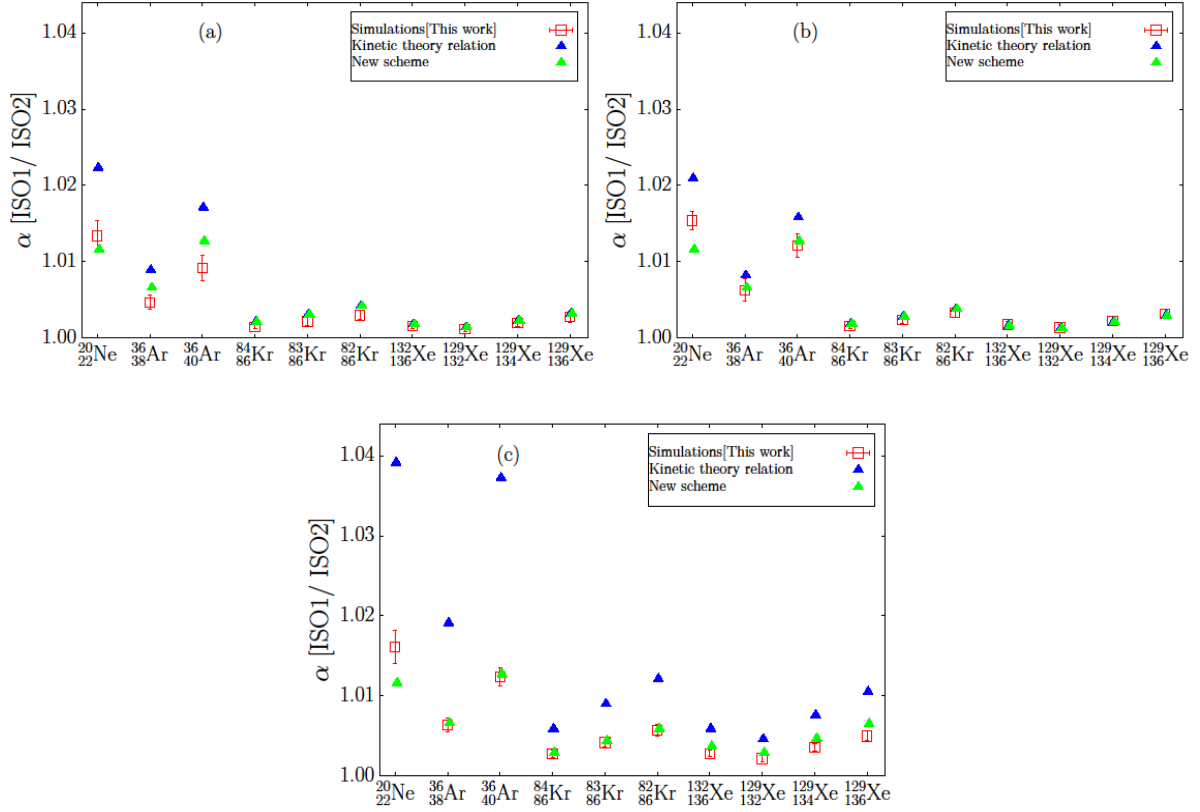
433

434 Thus, because of this simple relation between size and mass for noble gases, the
435 influence of the molecular radius on noble gases elemental fractionation, although dominating
436 in dense fluids, see equation (10), can be relatively well captured by considering the square
437 root law on mass only. This explains why, whatever the fluid regime, the square root law is
438 well suited to quantify noble gas elemental fractionation in geo-fluids, except for He.

439 **4.2. Isotopic Fractionation of Noble Gases**

440 In the following, to avoid an over-interpretation, the discussion is limited to Ne, Ar, Kr
441 and Xe isotope fractionation as the molecular simulations result is not consistent with the
442 experimental point for He in water, as indicated previously.

443 As can be deduced from Fig. 3 as well as from Figs. S2-S4 and clearly exhibited on
444 Fig. 4, the simulations results, and most previous experiments, showed that the square root
445 law is unable to correctly predict the isotopic fractionation of noble gases in water, as well as
446 in gas and oil. Interestingly, if one uses the kinetic theory relation, equation (5), suitable *a*
447 *priori* for both gas and dense gas regimes, the results are far better than those deduced from
448 the square root law, see Figs 4 and 6. More precisely, as shown on Figs. 6a and 6b and in
449 tables S6 and S7 (Supplementary Material), the kinetic theory relation is able to provide a
450 reasonable estimate of the noble gases isotopic fractionation in water and in gas, showing
451 nevertheless an increasing overestimation with the decrease of the studied noble gas
452 molecular mass. When considering the results in oil, see Fig. 6c and in table S8
453 (Supplementary Material), the kinetic theory relation tends to systematically overestimate the
454 fractionation by a factor of two or three.



455

456

457 *Figure 6: Isotopic fractionation of noble gases (without Helium) for classical noble gas*
 458 *isotopic ratios. ISO1 and ISO2 respectively stand for numerator and denominator noble gas*
 459 *isotope and α is the fractionation coefficient for ISO1/ISO2 ratio. (a) In water. (b) In a gas at*
 460 *$T=423$ K and $P = 50$ MPa. (c) In an oil at $T=323$ K and $P=10$ MPa.*

461

462 From the previous results, it seems that the deviations between the kinetic theory and
 463 molecular simulations data on isotope fractionation are related to the mass ratio between the
 464 noble gas and the solvent. More precisely, the deviations tend to increase when the molecular
 465 mass ratio between the considered noble gas and the solvent decreases. Thus, this indicates
 466 that a relation not dependent on the solvent molecular mass, such as equation (9), would fail
 467 to describe the noble gas isotopic fractionation in different geo-fluids. A more suitable
 468 relation would be of the following type:

469

$$\alpha[i/j] = \left(\frac{\mu_j}{\mu_i}\right)^\beta = \left(\frac{M_j}{M_i}\right)^\beta \times \left(\frac{M_i+M_s}{M_j+M_s}\right)^\beta \quad (16)$$

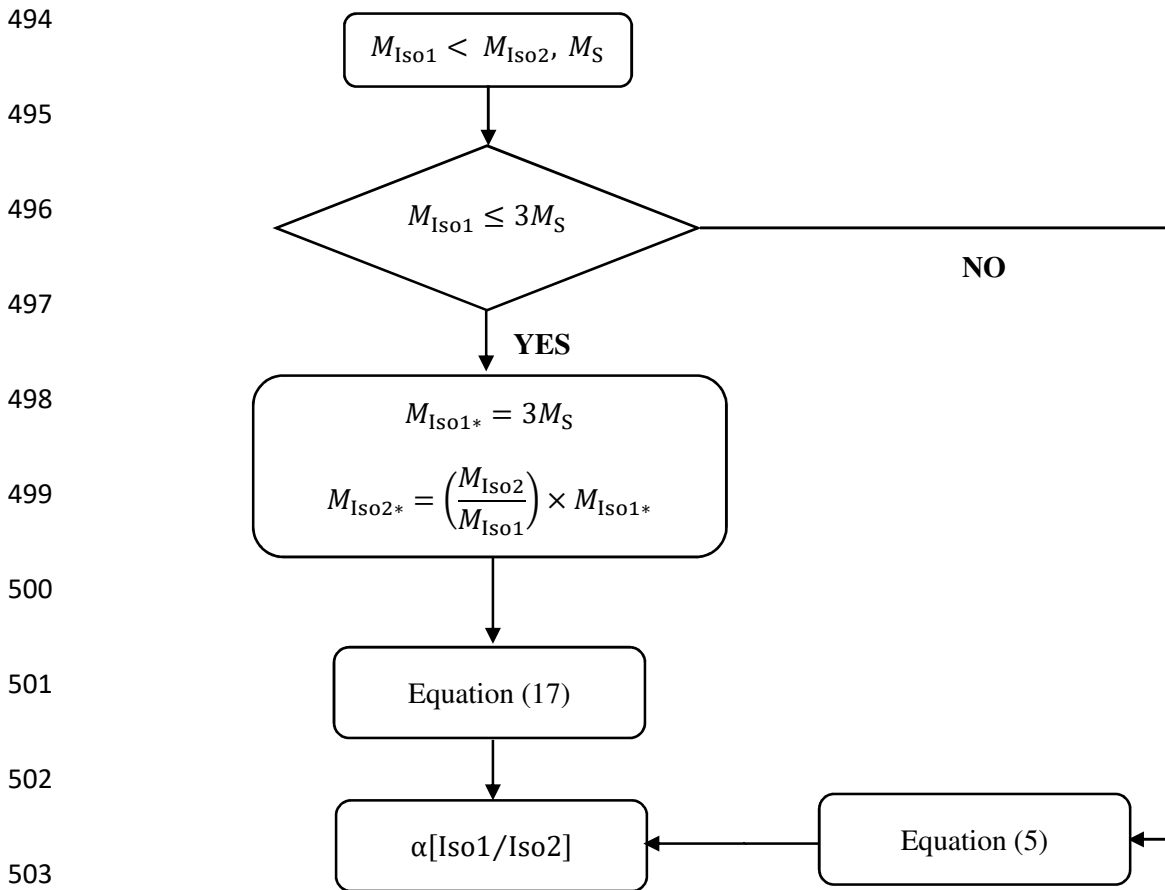
470 where β is a numerical parameter that may vary from $\frac{1}{2}$ to 0 (i.e. from the kinetic theory
 471 value, $\frac{1}{2}$, down to the Brownian dynamics one, 0) depending on both the diffusion regime and
 472 the molecular mass ratio between the considered noble gas and the solvent. However, from
 473 our results, the parametrization of β appears to be a complex function of the fluid regime and
 474 the solvent to noble gas molecular mass ratio preventing the possibility of building a simple
 475 predictive model based on eq. (16). So, to provide a practical and simple predictive model, the
 476 following semi-empirical approach is proposed to estimate fractionation between two noble
 477 gas isotopes, Iso1 and Iso2, Iso1 being the lightest one, in geo-fluids.

478 From Figs. 6a and 6b, it appears that, if the molecular mass of Iso1 is larger than about
 479 3 times that of the solvent, the kinetic theory (eq. 5) holds well. So, in such cases, equation (5)
 480 can directly be used. When $M_{\text{Iso1}} \leq 3M_s$, the idea is to define two isotopes of a “*theoretical*”
 481 noble gas element, named Iso1* and Iso2*, which presents the same molecular characteristics
 482 as a real noble gas (except He), as exhibited on Fig. 4. It is then possible to apply the square
 483 root law to estimate the “*elemental*” fractionation between the two isotopes of the noble gas of
 484 interest, Iso1 and Iso2, and those of the theoretical noble gas. This leads to $\alpha[\text{Iso1}^*/\text{Iso1}] =$
 485 $(M_{\text{Iso1}}/M_{\text{Iso1}^*})^{1/2}$ and $\alpha[\text{Iso2}^*/\text{Iso2}] = (M_{\text{Iso2}}/M_{\text{Iso2}^*})^{1/2}$. In addition, by imposing that
 486 $M_{\text{Iso2}^*}/M_{\text{Iso1}^*} = M_{\text{Iso2}}/M_{\text{Iso1}}$, one can deduce that $\alpha[\text{Iso1}/\text{Iso2}] = \alpha[\text{Iso1}^*/\text{Iso2}^*]$.
 487 Finally by choosing $M_{\text{Iso1}^*} = 3M_s < M_{\text{Iso2}^*}$, it is then possible to apply the kinetic theory (eq.
 488 5) to determine $\alpha[\text{Iso1}^*/\text{Iso2}^*]$ and so to deduce $\alpha[\text{Iso1}/\text{Iso2}]$. This leads to the following
 489 final relation:

$$490 \quad \alpha[\text{Iso1}/\text{Iso2}] = \left(\frac{M_{\text{Iso2}^*}}{M_{\text{Iso1}^*}}\right)^{\frac{1}{2}} \times \left(\frac{M_{\text{Iso1}^*} + M_s}{M_{\text{Iso2}^*} + M_s}\right)^{\frac{1}{2}} = \left(\frac{M_{\text{Iso2}}}{M_{\text{Iso1}}}\right)^{1/2} \times \left(\frac{4}{3 \times \frac{M_{\text{Iso2}}}{M_{\text{Iso1}}} + 1}\right)^{1/2} \quad (17)$$

491 For the sake of clarity, Fig. 6 provides a flowchart of the proposed scheme to estimate the
 492 isotopic fractionation of noble gases in geo-fluids.

493



504 *Figure 6: Flowchart of the proposed scheme to compute the isotopic fractionation of noble*
 505 *gases in geo-fluids.*

506

507 Noble gas isotopic fractionations predicted from the proposed scheme in water, gas
 508 and oil are provided respectively in Figs. -6a, 6b and 6c (data are provided in Tables S6, S7
 509 and S8 in the SM). Results clearly show that this scheme is able to yield results in good
 510 agreement with the simulation data whatever the geo-fluids. Compared to the kinetic theory
 511 relation, and even more to the square root law, the results are noticeably improved while
 512 keeping a purely predictive and a relatively simple scheme. This is further emphasized by the
 513 values of the self-diffusion coefficients deduced from the different relations compared to the
 514 simulation results, see Fig. 3 and Figs S1-S4.

515 **5. Conclusions**

516 In this work, we investigated the capability of theoretical models to predict the
517 elemental and isotopic kinetic fractionation of noble gases due to molecular diffusion in
518 geological fluids. First, a brief review of the available theoretical models depending on the
519 fluid conditions was presented. It was pointed out that, among them, the square-root law,
520 which is the most widely used approach, is theoretically valid only under the free molecular
521 regime, i.e. far from sub-surface conditions. To test the applicability domains of the different
522 fractionation models, we performed molecular dynamics simulations to compute the
523 elemental and isotopic fractionations of noble gases in water, gas (methane) and oil (n-
524 hexane) under subsurface conditions. Such simulations, which were found to provide results
525 in good agreement with experiments and previous simulations in water, were performed to
526 enlarge the geological fluids type on which the models could be tested.

527 Interestingly, the molecular simulation results evidenced that the noble gases
528 elemental fractionation can be quantitatively estimated by the square-root relation for the
529 major noble gas (^{20}Ne , ^{40}Ar , ^{84}Kr and ^{132}Xe) not only in water, as previously pointed out in the
530 literature from experiments and molecular simulations, but also in oil and in gas, except for
531 ^4He . This unexpected applicability of the square root relation is explained by a peculiar
532 relationship between the molecular mass and the molecular size for noble gases, thanks to the
533 kinetic theory. More precisely, the reciprocal of the square root of the molecular mass linearly
534 scales with the reciprocal of the square of the molecular size for (^{20}Ne , ^{40}Ar , ^{84}Kr and ^{132}Xe),
535 whereas it is not the case for ^4He .

536 Regarding the noble gas isotopic fractionation, it is confirmed, as recently shown in
537 the literature in water, that the square-root law is not able to predict good results in all studied
538 solvents. On the opposite, it was found that the kinetic theory relation has good predictive
539 capability in gas that deteriorates for denser solvents like oil and water.

540 Finally, to be able to quantify the noble gas isotopic fractionation in geological fluids,
 541 we have proposed a predictive scheme yielding results in good agreement with the simulation
 542 data and most of the experimental results. Compared to the square-root law and the kinetic
 543 theory relation, this scheme is noticeably better. As a summary of the previous findings, all
 544 fluid regime domains and corresponding relations to be applied are summarized in table 1.

545 *Table 1: Applicability domain for $\alpha \left[\frac{i}{j} \right]$ prediction of noble gases in geo-fluids.*

<i>Fluid regime</i>	<i>Elemental fractionation</i>	<i>Isotopic fractionation</i>
<i>Free molecular regime</i>	$\left(\frac{M_j}{M_i} \right)^{\frac{1}{2}}$	$\left(\frac{M_j}{M_i} \right)^{\frac{1}{2}}$
<i>Gas regime</i>		$\left(\frac{M_j}{M_i} \right)^{\frac{1}{2}} \times \left(\frac{M_j + M_s}{M_i + M_s} \right)^{\frac{1}{2}}$
<i>Dense gas regime and Liquid regime</i>		If $M_j > M_i \geq 3M_s$ $\left(\frac{M_j}{M_i} \right)^{\frac{1}{2}} \times \left(\frac{M_j + M_s}{M_i + M_s} \right)^{\frac{1}{2}}$
		If $M_i < 3M_s$ $\left(\frac{M_j}{M_i} \right)^{1/2} \times \left(\frac{4}{3 \times \frac{M_j}{M_i} + 1} \right)^{1/2}$

546

547

548 **Acknowledgements:**

549 We gratefully acknowledge TOTAL S.A. for the post-doctoral grant awarded to one of us
 550 (HH) and for letting us publish these results. We also thank the Pau University and the MCIA
 551 for providing computational facilities. Prof. Khac Hieu Ho would like to acknowledge

552 financial support from the Vietnam National Foundation for Science and Technology
553 Development (NAFOSTED) under grant number 103.01-2019.49.

554

555 **References**

556 Ali S. M., Samanta A.; Ghosh, S. K. (2001) Mode coupling theory of self and cross
557 diffusivity in a binary fluid mixture: Application to Lennard-Jones systems. *J. Chem. Phys.*
558 **114**, 10419-10429.

559 Allen, M. P., Tildesley D. J., (2017) *Computer simulation of liquids*. Oxford University Press.

560 Andersen H. C., (1983) Rattle: A “velocity” version of the shake algorithm for molecular
561 dynamics calculations. *J. Comput. Phys.* **52**, 24-34.

562 Ballentine C. J., Burgess R., and Marty B. (2002) Tracing fluid origin, transport and
563 interaction in the crust. *i* **47** (1), 539-614.

564 Berendsen H. J. C., Grigera J. R., and Straatsma T. P. (1987) The missing term in effective
565 pair potentials. *J. Phys. Chem.* **91**, 6269-6271.

566 Berendsen H. J., Postma J. V., van Gunsteren W. F., DiNola A. R. H. J., and Haak J. R.
567 (1984) Molecular dynamics with coupling to an external bath. *J. Phys. Chem.* **81**, 3684-3690.

568 Bhattacharyya S., and Bagchi B. (2000) Power law mass dependence of diffusion: a mode
569 coupling theory analysis. *Phys. Rev. E* **61**, 3850.

570 Bourg I. C. and Sposito G. (2008) Isotopic fractionation of noble gases by diffusion in liquid
571 water: Molecular dynamics simulations and hydrologic applications. *Geochim. Cosmochim.*
572 *Acta* **72**, 2237-2247.

573 Bourg I. C., Richter F. M., Christensen J. N. and Sposito G. (2010) Isotopic mass dependence
574 of metal cation diffusion coefficients in liquid water. *Geochim. Cosmochim. Acta* **74**, 2249–
575 2256.

576 Burnard P. (2013) *The noble gases as geochemical tracers*. New York: Springer.

577 Chapman S. and Cowling T. G. (1970) *The Mathematical Theory of Non-Uniform Gases*,
578 Cambridge Univ. Press, Cambridge.

579 Cussler E. L. (2009) *Diffusion: Mass Transfer in Fluid Systems*. Third Edition, Cambridge
580 University Press, New York.

581 de Magalhães H.P., Brennwald M.S. and Kipfer, R. (2017) Diverging effects of isotopic
582 fractionation upon molecular diffusion of noble gases in water: mechanistic insights through
583 ab initio molecular dynamics simulations. *Environ. Sci.: Processes Impacts* **19**, 405-413.

584 Deserno M. and Holm C. (1998) How to mesh up Ewald sums. II. An accurate error estimate
585 for the particle–particle–particle-mesh algorithm. *J. Chem. Phys.* **109**, 7694-7701.

586 Frenkel, D. and Smit B. (2001) *Understanding molecular simulation: from algorithms to*
587 *applications*, Second Edition, Academic Press.

588 Galliero G., Bataller H., Bazile J. P., Diaz J., Croccolo F., Hoang H., Vermorel R., Artola
589 P.A., Rousseau B., Vesovic V., Bou-Ali M., de Zarate J.M.O., Xu S., Zhang K., Montel F.,
590 Verga A., and Minster O. (2017) Thermodiffusion in multicomponent n-alkane mixtures. *npj*
591 *Microgravity* **3**, 1-7.

592 Gunn R. D., Chueh P. L., and Prausnitz, J. M. (1966). Prediction of thermodynamic properties
593 of dense gas mixtures containing one or more of the quantum gases. *AIChE J.* **12**, 937-941.

594 Hamani A. W. S., Bazile J. P., Hoang H., Luc H. T., Daridon J. L., and Galliero G. (2020)
595 Thermophysical properties of simple molecular liquid mixtures: On the limitations of some
596 force fields. *J. Mol. Liq.* (303) 112663.

597 Hoang H., Delage-Santacreu S., and Galliero G. (2017) Simultaneous description of
598 equilibrium, interfacial, and transport properties of fluids using a Mie chain coarse-grained
599 force field. *Ind. Eng. Chem. Res.* **56**, 9213-9226.

600 Hoang H., Nguyen P., Pujol M., and Galliero G. (2019) Elemental and isotopic fractionation
601 of noble gases in gas and oil under reservoir conditions: Impact of thermodiffusion. *Eur.*
602 *Phys. J. E* **42**, 61.

603 Hirschfelder J. O., Curtiss C. F. and Bird R. B. (1954) *Molecular theory of gases and liquids*.
604 Wiley, New York.

605 Holz M., Haselmeier R., Mazitov R. K., and Weingaertner H. (1994) Self-diffusion of neon in
606 water by ^{21}Ne NMR. *J. Am. Chem. Soc.* **116**, 801-802.

607 Jähne B., Heinz G. and Dietrich W. (1987) Measurement of the diffusion coefficients of
608 sparingly soluble gases in water. *J. Geophys. Res. Oceans* **92**, 10767-10776.

609 Kincaid J. M., Perez S., and Cohen E. G. D. (1988) Modified Enskog theory for fluid
610 mixtures. *Phys. Rev. A* **38**, 3628.

611 Kincaid J. M., Tuo R. F. and Lopez de Haro M. (1994) A test of the modified Enskog theory
612 for self-diffusion. *Mol. Phys.* **81**, 837-850.

613 Leach A. R. (2001) *Molecular Modelling: Principles and Applications*. Second Edition,
614 Prentice Hall, Harlow.

615 Marrink S. J. and Tieleman D. P. (2013) Perspective on the Martini model. *Chem. Soc. Rev.*
616 **42**, 6801-6822.

617 Martin M. G. and Siepmann J. I. (1998) Transferable potentials for phase equilibria. 1.
618 United-atom description of n-alkanes. *J. Phys. Chem. B* **102**, 2569-2577.

619 Marty B. (1984) On the noble gas, isotopic fractionation in naturally occurring gases.
620 *Geochem. J.* **18**, 157-162.

621 Ozima, M. and Podosek F. A. (2002) *Noble gas geochemistry*. Cambridge. University Press.

622 Panagiotopoulos A. Z. (1989) Exact calculations of fluid-phase equilibria by Monte Carlo
623 simulation in a new statistical ensemble. *Int. J. Thermophys.* **10**, 447-457.

624 Plimpton S. 1995. Fast parallel algorithms for short-range molecular dynamics. *J. Comput.*
625 *Phys.* **117**, 1-19.

626 Poling, B. E. Prausnitz J. M. and O'connell J. P. (2001) *The Properties of Gases and Liquids*,
627 Fifth Edition, New York: Mcgraw-Hill.

628 Prinzhofer A., Vega M.A.G, Battani A. and Escudero M. (2000) Gas geochemistry of the
629 Macuspana Basin (Mexico): thermogenic accumulations in sediments impregnated by
630 bacterial gas, *Mar. Pet. Geol.* **17**, 1029-1040.

631 Richter F. M., Mendybaev R. A., Christensen J. N., Hutcheon I. D., Williams R. W., Sturchio
632 N. C. and Beloso Jr. A. D. (2006) Kinetic isotopic fractionation during diffusion of ionic
633 species in water. *Geochim. Cosmochim. Acta* **70**, 277–289.

634 Ross J.J. (2018) A literature survey of noble gas solubility measurements in formation brines
635 to interpret tracer experiments, Bachelor's Thesis, Ohio State University.

636 Samanta A., Ali S. M., and Ghosh S. K. (2001) Universal scaling laws of diffusion in a binary
637 fluid mixture. *Phys. Rev. Lett.* **87**, 245901.

638 Samanta A., Ali S. M. and Ghosh S. K. (2004) New universal scaling laws of diffusion and
639 Kolmogorov-Sinai entropy in simple liquids. *Phys. Rev. Lett.* **92**, 145901.

640 Seltzer A. M., Ng J. and Severinghaus J. P. (2019) Precise determination of Ar, Kr and Xe
641 isotopic fractionation due to diffusion and dissolution in fresh water. *Earth Planet. Sci. Lett.*
642 **514**, 156-165.

643 Siu S. W., Pluhackova K. and Böckmann R. A. (2012) Optimization of the OPLS-AA force
644 field for long hydrocarbons. *J. Chem. Theory Comput.* **8**, 1459-1470.

645 Tempest K. E. and Emerson S. (2013) Kinetic isotopic fractionation of argon and neon during
646 air–water gas transfer. *Mar. Chem.* **153**, 39-47.

647 Tyroller L., Brennwald M. S., Busemann H., Maden C., Baur H., and Kipfer R. (2018)
648 Negligible fractionation of Kr and Xe isotopes by molecular diffusion in water. *Earth Planet.*
649 *Sci. Lett.* **492**, 73-78.

650 Tyroller L., Brennwald M. S., Mächler L., Livingstone D. M. and Kipfer R. (2014)
651 Fractionation of Ne and Ar isotopes by molecular diffusion in water. *Geochim. Cosmochim.*
652 *Acta* **136**, 60-66.

653 Verlet L. (1967) Computer" experiments" on classical fluids. I. Thermodynamical properties
654 of Lennard-Jones molecules. *Phys. Rev.* **159**, 98.

655 Wanner P. and Hunkeler D. (2019) Isotope fractionation due to aqueous phase diffusion–
656 What do diffusion models and experiments tell? - A review. *Chemosphere* **219**, 1032-1043.

657 Warr O., Ballentine C. J., Mu J., and Masters A. (2015) Optimizing Noble Gas–water
658 interactions via Monte Carlo simulations. *J. Phys. Chem. B* **119**, 14486-14495.

659 Watkins J. M., DePaolo D. J. and Watson E. B. (2017) Kinetic fractionation of non-traditional
660 stable isotopes by diffusion and crystal growth reactions. *Rev. Mineral. Geochem.*, **82**, 85-
661 125.

662 Wilke C. R. and Chang P. (1955) Correlation of diffusion coefficients in dilute solutions.
663 *AIChE J.* **1** 264-270.

664 Zeebe R. E. (2011) On the molecular diffusion coefficients of dissolved CO₂, HCO₃⁻ and CO₃²⁻
665 and their dependence on isotopic mass. *Geochim. Cosmochim. Acta* **70**, 277–289.